Ground Motion in Kuwait from Regional and Local Earthquakes: Potential Effects on Tall Buildings

As Published: https://doi.org/10.1007/s00024-018-1943-5

Publisher: Springer International Publishing

Ground Motion in Kuwait from Regional and Local Earthquakes: Potential Effects on Tall Buildings

Chen Gu[1], Germán A Prieto[4], Abdullah Al-Enezi[3], Farah Al-Jeri[3], Jamal Al-Qazweeni[3], Hasan Kamal[3], Sadi Kuleli[1], Aurélien Mordret[1], Oral Büyüköztürk[2], M. Nafi Toksöz[1]

[1]Earth Resources Laboratory, Department of Earth, Atmospheric, and Planetary Sciences, Massachusetts Institute of Technology, Cambridge, MA, USA.

[2]Laboratory for Infrastructure Science and Sustainability, Department of Civil and Environmental Engineering, Massachusetts Institute of Technology, Cambridge, MA, USA.

[3]Kuwait Institute for Scientific Research, Kuwait City, Kuwait.

[4]Departamento de Geociencias, Facultad de Ciencias, Universidad Nacional de Colombia, Bogotá, Colombia

Abstract In recent years, the construction of tall buildings has been increasing in many countries, including Kuwait and other Gulf states. These tall buildings are especially sensitive to ground shaking due to long period seismic surface waves. Although Kuwait is relatively aseismic, it has been affected by large (Mw > 6) regional earthquakes in the Zagros Fold-Thrust Belt (ZFTB). Accurate ground motion prediction for large earthquakes is important to assess the seismic hazard to tall buildings. In this study, we first analyze the observed ground motions due to two earthquakes widely felt in Kuwait: the 08/18/2014 Mw 6.2 earthquake, 360 km NNE of Kuwait City, and the 11/12/2017 Mw 7.3 earthquake, 642 km NNE of Kuwait City. The peak spectral displacement periods of the ground motion from the 08/18/2014 Mw 6.2 earthquake matched well with the ambient vibration spectra of the tallest building - the Al-Hamra Tower. We calculate the ground motions from potential regional and local earthquakes. We use a velocity model obtained by matching the observed seismograms of the 2014 and 2017 earthquakes. We calculate ground motions in Kuwait due to a regional Mw = 7.5 earthquake, and a local Mw = 5.0 earthquakes. Our study shows that a significant source of seismic hazard to tall buildings in Kuwait comes from the regional tectonic earthquakes. However, local earthquakes have the potential to generate high peak ground accelerations (~ 98 cm/sec^2) close to their epicenters.

1. Introduction

There has been a rapid increase in the total number and construction of tall buildings worldwide, including in Kuwait. Tall buildings are greatly affected by long trains of low-frequency seismic surface waves from regional earthquakes. Ground motions from regional large earthquakes have frequency contents that may be in the same range as the natural frequencies of some of these tall buildings; and this may have damaging consequences (Shakal et al., 1996; Çelebi and Liu, 1998; Çelebi et al., 2014). The building response to seismic shaking may be obtained by seismic interferometry using ambient vibrations or recorded earthquakes from the building monitoring system (Kohler et al., 2005; Snieder and Şafak, 2006; Prieto et al., 2010; Sun et al., 2017).

Previous studies used different methods to calculate the ground motion in a region (Abrahamson and Shedlock, 1997; Olsen et al., 1995; Pitarka et al., 1998; Olsen, 2000; Olsen et al., 2006, 2009; Prieto and Beroza, 2008; Denolle et al., 2013, 2014). The ground motion prediction equation (GMPE) is one method to estimate ground motion intensity based on the observed seismic data and attenuation laws (Abrahamson and Shedlock, 1997; Cauzzi et al., 2014; Danciu et al., 2017, 2018; Şeşetyan et al., 2018). However, in many areas with limited information this approach is primarily directed to acceleration and does not include long period surface waves and the earthquake source rupture process, especially important for large earthquakes; it also ignores the effects of regional variations in crustal structures along the wave propagation path. To make the prediction more physical and realistic, many studies use numerical methods to predict ground motions from a simulated large earthquake (Olsen et al., 1995; Pitarka et al., 1998; Olsen, 2000; Olsen et al., 2006, 2009). The reliability of these ground motion simulations depends heavily on the accuracy of the earthquake source rupture model and the velocity and attenuation models used to propagate seismic waves. In the last decade, studies have started using the ambient seismic field to predict the ground motions from sources around seismic stations (Prieto and Beroza, 2008; Denolle et al., 2013, 2014). This method, although appealing, is limited because it only predicts the ground motions near available seismic stations and thus requires a high-density network. In this report, we use numerically simulated ground motions for both regional and local earthquakes in and near Kuwait.

Ground motion predictions in Kuwait are possible thanks to well-documented studies on regional tectonics, earthquake source mechanisms and seismic velocity structures in and around Kuwait. These data provide the starting models for the ground motion calculations (Jackson and McKenzie, 1984; Ni and Barazangi, 1986; Bou-Rabee, 2000; Gök et al., 2000; Talebian and Jackson, 2004; Pasyanos et al., 2007; Sadek, 2008; Abbas and Al-Sabri, 2015; Kottmeier et al., 2016; Çaktı et al., 2016). In addition, some previous research has been conducted on long-period ground motions in the Arabian Gulf (Pitarka et al., 2012, 2015). El-Hussain et al. (2012, 2013, 2015) carried out extensive studies of earthquake catalogs for the Zagros Fold-Thrust Belt (ZFTB) and Gulf region as part of their study of seismic hazard in Oman. In the State of Kuwait, hazard studies have been confined mostly to local regions and earthquakes (Bou-Rabee, 2000).

In this paper, we calculate ground motions from large regional earthquakes around Kuwait, mostly in the ZFTB and from the largest local earthquakes in Kuwait. To minimize uncertainties associated with crustal and sedimentary basin structures, we determine a regional velocity model using data from two regional earthquakes, 08/18/2014 Mw 6.2 and 11/12/2017 Mw 7.3, recorded by seismic stations in Kuwait. To deterministically address seismic hazard from regional earthquakes in Kuwait City, we simulate ground motions from a Mw = 7.5 regional earthquake, located 300 km east of Kuwait City. The response spectra (spectral displacement/pseudo-acceleration spectra) are also calculated and compared with the mode vibrations obtained from ambient vibrations spectra of the Al-Hamra Tower to assess the seismic hazard to tall buildings in Kuwait City. In addition, the ground motions due to recent local earthquakes are calculated.

2. Ground Motion Data and Model

The Kuwait National Seismic Network (KNSN), started in 1997, has been monitoring earthquakes since then (Figure 2b). The KNSN initially consisted of seven three-component short-period stations (AB, MI, QR, RD, RS, SA, UM) and one three-component broadband station (KB). In 2013, the KNSN upgraded their seismic monitoring network by replacing five short-period stations (MI, QR, RD, RS, UM) with broadband stations (RefTek's 151-120 broadband seismometers with a natural period of 120 sec). In this study, we use only the broadband seismic data, since the instrument response files for short-period stations AB and SA are not available. We deconvolve the instrument response from the raw digital data to convert them to ground velocity seismograms. A quarter-cycle cosine taper, with unit response between 0.0125 Hz and 8.0 Hz and zero below 0.01 Hz and above 10.0 Hz, was applied during the deconvolution to dampen the response at very low and high frequencies. The displacement and acceleration seismograms are obtained by integrating and differentiating the velocity seismograms, respectively. The spectral displacement, pseudo-velocity spectra and pseudo-acceleration spectra are calculated to estimate the potential effects of earthquakes on civil structures (Gupta, 1992).

To calculate the ground motion, we used the discrete-wavenumber method (Bouchon, 1981; 2003). This method, which converts the continuous wavenumber integration to a summation of discrete wavenumbers, is an accurate and computationally efficient method for generating synthetic seismograms for a 1-D layered velocity model. We could have used a finite difference method for 2-D or 3-D velocity models if such models were available (Olsen, 2000; Olsen et al., 2006; Maeda and Furumura, 2013; Almuhaidib and Toksöz, 2014).

The 1-D layered velocity model we used is based on the KUW1 model of Pasyanos et al. (2007). The KUW1 model was modified to include the sedimentary layers and fit the observed seismograms from the two large earthquakes in 2014 and 2017. The new model, designated KUW-P or preferred model, is listed in Table 1 and shown in Figure 3. More detailed velocity model improvement procedure is included in the supplemental materials. The large regional earthquakes occur mostly in the Zagros Fold-Thrust Belt (ZFTB) and surrounding areas (Pasyanos et al., 2007; Sadek, 2008). Figure 1 shows significant regional earthquakes around Kuwait in the period 1997-2017. On average, about one earthquake of magnitude 6 or greater occurs in the region per year. In Figure 1, we also show sample seismograms (vertical components) recorded at station MI. Unfortunately, the length of the recordings is limited to 200 seconds and seismograms are truncated. For closer events (e.g. at about 300 km distance), we note the long duration of surface waves.

The observed long-period, long-duration ground motion in Kuwait shows that regional earthquakes are one source of hazards to tall buildings in Kuwait. To demonstrate the impact of regional earthquakes on tall buildings in Kuwait, we analyze seismograms from two large Zagros belt earthquakes that occurred in 2014 and 2017.

The 08/18/2014 Mw 6.2 earthquake, which happened at the Iran-Iraq border, 360 km NNE of Kuwait City, was widely felt in Kuwait. We show the three-component seismograms of this earthquake from four stations in Kuwait and RAYN in Saudi Arabia in Figure 2. Since this earthquake occurred to the north of Kuwait and from station RYAN in Saudi Arabia, the Z and N component seismograms are alike and are with a 90-degree phase shift, mostly Rayleigh waves. The seismograms at the station RD and QR in Kuwait are truncated because the recordings were limited to 200 secs. The E component is primarily Love waves.

To calculate synthetic seismograms, we use a 1-D layered velocity model (KUW-P). The comparison between the observed and calculated seismograms for the Mw 6.2 are shown in Figure 4. The figure also includes the spectral displacements. The peak displacement response peaks at periods 3.4 s, 6.9 s, and 16.0 s are due to shear, Rayleigh and Love waves, respectively.

We do the similar comparison of synthetic and observed seismograms for the recent 11/12/2017 Mw 7.3 earthquake, 642 km NNE of Kuwait City, at the Iran-Iraq border. The comparison of the observed and modeled ground displacements and spectral displacements of the Mw 7.3 earthquake at stations KB, QR and RS is shown in Figure 5. The horizontal components of broad band recordings were slightly clipped due to the large magnitude. In spite of this, the match between the observed displacement seismograms and spectral displacements is good, especially for the vertical components least impacted by the clipping. The peak spectral displacements are above 10 s period. The peak ground displacement is about 4 cm and the duration of the ground motions is longer than 300 sec.

3. Ground Motions in Kuwait Due to Regional and local Earthquakes

The determination of ground motion requires the maximum credible magnitude, source properties and the most likely locations. For Kuwait, the primary site for a regional earthquake is the segment of the ZFTB, 300 km east of the Kuwait City. The maximum credible magnitude is Mw = 7.5, based on the regional earthquake catalog from the KNSN and the work of El-Hussain et al. (2012, 2013), who have conducted extensive studies of regional earthquakes in the ZFTB for seismic hazard zonation in the Sultanate of Oman. A Mw = 7.5 earthquake corresponds to a moment of $M_0 = 2.24 \times 10^{27}$ dyne □ cm. In our calculation, source (fault rupture area) was assumed to be 20 km × 40 km with the top of the rupture 5 km below the surface. The modeled earthquake is a thrust event with fault plane: strike = 300°, dip = 20°, and rake = 90°. Using the KUW-P velocity model (Table 1), we calculate synthetic seismograms with the epicenter located 300 km east of Kuwait City.

The calculated ground accelerations and displacements in Kuwait are shown in Figure 6. Our calculations show that in Kuwait City, the maximum acceleration is 46 cm/sec^2 and maximum displacement is 23 cm. The peaks of the displacement response spectra are above 10 s period. The duration of the ground motion is longer than 300 seconds.

To demonstrate the effects of ground motions in Kuwait due to regional earthquakes on tall buildings in Kuwait City, we look at the Al-Hamra Tower. The Al-Hamra Tower is a 414 m tall sculpted concrete steel structure. The resonant frequencies of the tower were obtained by finite element modeling and by ambient vibrations measurements. For the ambient vibrations monitoring, Kuwait Institute for Scientific Research (KISR) deployed two accelerometers at the top terrace of the Al-Hamra Tower in Kuwait City (two Kinemetrics systems, with 3-component Episensor and Q330 dataloggers). We used ambient vibrations to obtain vibration spectra of the Al-Hamra Tower on day 329 of 2013, shown in Figure 7.

The peak periods obtained from the two instruments are quite consistent. The periods of the first and second strongest building spectral peaks (7.1 sec and 5.7 sec) are close to the calculated peak spectral displacement shown in Figure 4. This overlap between the dominant frequency of ground motions from regional earthquakes, similar to the Mw 6.2 earthquake, and the natural frequencies of the Al-Hamra Tower suggests that regional earthquakes will cause strong resonance vibrations in the Al-Hamra Tower and other tall buildings of similar height. The observed ground motions due to the Mw 7.3 earthquake, 642 km from Kuwait City, have large (about 4 cm) amplitudes at periods less the 10 sec, but the peak displacement response periods are larger than 10 sec; however, the large peak ground displacements, ~4 cm due to the Mw 7.3 earthquake could still cause large motions at the higher floors of the building. The observed building motions due to the Mw 7.3 earthquake from the first GPS measurements of the Al-Hamra tower (Herring et al., 2018, submitted) indicate a building displacement of ~20 cm at the top of the 414 m tall building. This amount of motion did not cause any damage to the Al-Hamra tower.

It is important to mention that the calculated ground motions shown in the figures are for a competent rock layer with shear velocity of 1.4 km/sec. “Soft” sediments with lower shear velocity would further amplify the ground motions. More detailed geotechnical information about the soil properties and sedimentary structures at the site are needed to better quantify and predict the ground motions (Bowden and Tsai, 2017). However, this is beyond the scope of this paper.

Local earthquakes in Kuwait occur frequently but tend to have small magnitudes (Pasyanos, 2007). Since 1997, the KNSN has recorded more than 1000 earthquakes (Mw < 5). Most of the local earthquakes are distributed close to the oil/gas fields in the northeast and southwest of Kuwait (Figure 8) and are probably induced by oil production activities (Gu et al., 2017). Two of the largest local earthquakes - Mw 4.5 on 03/21/2015 and Mw 4.1 on 08/18/2015 - are located near the southern oil fields and near the northern oil fields, respectively. Such seismicity related to oil/gas fields has also been observed in North America, Europe and the Middle East (Sarkar, 2008; Li et al., 2011a, b; Zoback and Gorelick, 2012; Ellsworth, 2013; Shapiro, 2015; Rubinstein, 2015; Bommer et al., 2017).

The seismograms of the Mw 4.5 earthquake from three selected stations and the corresponding pseudo acceleration response spectra are shown in Figure 9. The peak acceleration response periods are in the range from 0.1 s to 1 s (10 Hz to 1 Hz).

So far, no earthquakes of magnitude greater than Mw 4.5 have been recorded in Kuwait. To determine the ground motions due to the largest local earthquake in Kuwait, we assumed a maximum credible magnitude Mw 5.0. We generated 3-compoment synthetics for a local Mw 5.0 earthquake at depth of 3 km (see Figure

10), with a reverse fault and source mechanism (strike = 85°, dip = 20°, and rake = 10°) that are consistent with regional stress (Carman, 1996; El-Hussain et al., 2012, 2015; Abbes and Al-Sabri, 2015; Gu et al., 2017). Figure 10 shows the peak ground acceleration (PGA), representing the root mean square (RMS) of the east and north components. Unlike the large regional earthquakes, the local earthquakes, which excite short period ground motions, would not affect the tall buildings. These earthquakes could generate accelerations (~ 98 cm/sec^2) high enough to affect small structures, built without seismic design codes. Because of the shallow depths, the maximum shaking generates high ground motions but is confined to a small area around these local earthquakes with a steep fall-off. Note that the maximum frequencies for the synthetics are 2Hz, this frequency limitation may under-estimate the PGA.

4. Conclusions

For tall buildings and large structures in Kuwait, the primary hazard is due to regional earthquakes (e.g., from Zagros Fold-Thrust Belt), especially from surface waves. Our ground motion calculation shows a maximum acceleration of 46 cm/sec^2 and a maximum displacement of 23 cm in Kuwait City from a virtual Mw 7.5 earthquake in the Zagros region. The presence of near surface “soft” layers increases duration and amplitudes of the surface waves (site amplification) and, hence, increases the hazard. Knowing the detailed shallow structure at the building site would help to better estimate the seismic site specific ground motions.

The local earthquakes, most likely induced by oil/gas field activities, can also represent seismic hazard (Gu et al., 2017). They can generate high peak ground accelerations (~ 0.1g) at periods less than 1 second, close to their epicenters. These local earthquakes may potentially affect local structures.

Acknowledgements

This project was sponsored by the Kuwait Foundation for the Advancement of Sciences. The project was conducted as part of the Kuwait-MIT signature project on sustainability of Kuwait’s built environment under the direction of Oral Büyüköztürk.

REFERENCES

Abbas, M. and N. A. Al-Sabri (2015). Focal mechanism and stress tensor analysis in the south Red Sea, *9th Gulf Seismic Forum*.

Abrahamson, N., and K. Shedlock (1997). Overview of ground motion attenuation relationships. *Seismol. Res. Lett.*, 68(1).

Anderson, S. and R. E. Grimm (1998). Rift processes at the Valles Marineris: Constraints from gravity on necking and rate-dependent strength evolution. *J. Geophys. Res., 103*, 11113-11124.

Almuhaidib, A. M., and M.N. Toksöz (2014). Numerical modeling of elastic-wave scattering by near-surface heterogeneities. *Geophysics*, 79(4), T199–T217.

Bommer, J. J., P. J. Stafford, B. Edwards, B. Dost, E. van Dedem, A. Rodriguez-Marek, P. Kruiver, J. van Elk, D. Doornhof, and M. Ntinalexis (2017). Framework for a Ground-Motion Model for Induced Seismic Hazard and Risk Analysis in the Groningen Gas Field, The Netherlands. *Earthquake Spectra*, Vol. 33, No. 2, pp. 481-498.

Bou-Rabee, F. (1999). Site selection for the field stations of the Kuwait National Seismic Network, *Seismol. Res. Lett.*, 70(6), 712–717.

Bou-Rabee, F. (2000). Seismotectonics and earthquake activity of Kuwait. *J. Seismol.*, 4(2), 133–141.

Bouchon, M. (1981). A simple method to calculate green's functions for elastic layered media. *Bull. Seismol. Soc. Am.*, 71(4), 959–971.

Bouchon, M. (2003). A review of the discrete wavenumber method. *Pure. and Appl. Geophy.*, 160(3-4), 445–465.

Bowden, D. C., and V. C. Tsai (2017). Earthquake ground motion amplification for surface waves. *Geophys. Res. Lett.*, 44, 121-127, doi:10.1002/2016GL071885.

Çaktı, E., I. El-Hussain, K. Şeşetyan, A. Deif, U. Hancılar, G. Al-Rawas, Y. Kamer & Al-Jabri, K. (2016). Development of ground-shaking maps for the Sultanate of Oman. *Nat. Hazards*, 82(2), 1357-1373.

Carman, G. J. (1996). Structural elements of onshore Kuwait. *GeoArabia*, 1, no. 2, 239–266.

Cauzzi, C., Faccioli, E., Vanini, M., & Bianchini, A. (2015). Updated predictive equations for broadband (0.01-10 s) horizontal response spectra and peak ground motions, based on a global dataset of digital acceleration records. *Bull. Earthquake Eng.*, 13(6), 1587.

Çelebi, M., and H.-P. Liu (1998). Before and after retrofit–response of a building during ambient and strong motions. *J. Wind Eng. Ind. Aerodyn.*, 204 77, 259–268.

Çelebi, M., M. N. Toksöz, and O. Büyüköztürk (2014). Rocking behavior of an instrumented unique building on the MIT campus identified from ambient shaking data. *Earthq. Spectra*, 30(2), 705–720.

Danciu, L., Kale, Ö., & Akkar, S. (2016), The 2014 Earthquake Model of the Middle East: ground motion model and uncertainties. *Bull. Earthquake Eng.*, 1-37.

Giardini, D., Danciu, L., Erdik, M., Şeşetyan, K., Tümsa, M. B. D., Akkar, S., ... & Zare, M. (2018), Seismic hazard map of the Middle East. *Bull. Earthquake Eng.*, 1-4.

Denolle, M., E. Dunham, G. Prieto, and G. Beroza (2013). Ground motion prediction of realistic earthquake sources using the ambient seismic field. *J. Geophy. Res.: Solid Earth*, 118(5), 2102–2118.

Denolle, M., E. Dunham, G. Prieto, and G. Beroza (2014). Strong ground motion prediction using virtual earthquakes. *Science*, 343(6169), 399–403.

Dziewonski, A. M., T.-A. Chou and J. H. Woodhouse (1981). Determination of earthquake source parameters from waveform data for studies of global and regional seismicity. *J. Geophys. Res.*, 86, 2825-2852.

El-Hussain, I., A. Deif, K. Al-Jabri, M. N. Toksoz, S. El-Hady, S. Al-Hashmi, K. Al-Toubi, Y. Al-Shijbi, M. Al-Saifi, S. Kuleli (2012). Probabilistic seismic hazard maps for the sultanate of Oman. *Nat. hazards*, 64(1), 173-210.

El-Hussain, A. Deif, K. Al-Jabri, A. M. E. Mohamed, G. Al-Rawas, M. N. Toksöz, N. Sundararajan, S. El-Hady, S. Al-Hashmi, K. Al-Toubi, M. Al-Saifi, Z. Al-Habsi, (2013). Seismic microzonation for Muscat region. Sultanate of Oman. *Nat. hazards*, 69(3), 1919-1950.

El-Hussain, I., A. Deif, A. M. E. Mohamed, K. Al-Jabri, B. Gareth, H. Yaqoup (2015). Deterministic seismic hazard assessment close to a gas field in northern Oman. *Arab J Geosci*, 8(7), 4299-4316.

Ekström, G., M. Nettles, and A. M. Dziewonski. The global CMT project 2004-2010: Centroid-moment tensors for 13,017 earthquakes. *Phys. Earth Planet. Inter.*, 200-201, 1-9, 2012.

Gök, R., N. Türkelli, E. Sandvol, D. Seber, and M. Barazangi (2000). Regional wave propagation in Turkey and surrounding regions. *Geophy. Res. Lett.*, 27(3), 429-432.

Gu, C., F. Al-Jeri, A. Al-Enezi, Oral Büyüköztürk, M.N. Toksöz (2017). Source mechanism study of local earthquakes in Kuwait. *Seismol. Res. Lett.*, 88(6), 1465-1471.

Gupta, A. K. (1992). Response spectrum method in seismic analysis and design of structures (Vol. 4). CRC press.

Herring, T. A., C. Gu, M. N. Toköz, O. Büyüköztürk, J. Parol, A. Enezi, F. Al-Jeri, J. Al-Qazweeni, H. Kamal (2018). GPS Measurements of Large Oscillations of a Tall Building Due to a Magnitude 7.3 Earthquake. submitted.

Jackson, J., and D. McKenzie (1984). Active tectonics of the Alpine—Himalayan belt between western Turkey and Pakistan, *Geophys. J. Int.*, 77(1), 185–264.

Kohler, M. D., P. M. Davis, and E. Safak (2005). Earthquake and ambient vibration monitoring of the steel-frame UCLA Factor Building, *Earthquake Spectra*, 21(3), 715–736.

Kottmeier, C., A. Agnon, D. Al-Halbouni, P. Alpert, U. Corsmeier, T. Dahm, ... & N. Kalthoff (2016). New perspectives on interdisciplinary earth science at the Dead Sea: The DESERVE project. *Science of the Total Environment*, 544, 1045-1058.

Maeda T., and Furumura T. (2013). FDM simulation of seismic waves, ocean acoustic waves, and tsunamis based on tsunami-coupled equations of motion[J]. *Pure Appl. Geophys.*, 170(1-2): 109-127.

Li, J., H. S. Kuleli, H. Zhang, and M. N. Toksöz (2011a). Focal mechanism determination of induced microearthquakes in an oil field using full waveforms from shallow and deep seismic networks, *Geophysics*, 76, no. 6, WC87–WC101.

Li, J., H. Zhang, H. S. Kuleli, and M. N. Toksöz (2011b). Focal mechanism determination using high-frequency waveform matching and its application to small magnitude induced earthquakes, *Geophys. J. Int.*, 184, no. 3, 1261–1274.

Ni, J., and Barazangi, M. (1986). Seismotectonics of the Zagros continental collision zone and a comparison with the Himalayas. *J. Geophy. Res.: Solid Earth*, 91(B8), 8205-8218.

Olsen, K. (2000). Site amplification in the Los Angeles basin from three-dimensional modeling of ground motion. *Bull. Seismol. Soc. Am.*, 90(6B), S77–S94.

Olsen, K., S. Day, J. Minster, Y. Cui, A. Chourasia, M. Faerman, R. Moore, P. Maechling, and T. Jordan (2006). Strong shaking in Los Angeles expected from southern San Andreas earthquake. *Geophy. Res. Lett.*, 33(7).

Olsen, K., S. Day, L. Dalguer, J. Mayhew, Y. Cui, J. Zhu, V. M. Cruz-Atienza, D. Roten, P. Maechling, T. H. Jordan, D. Okaya, A. Chourasia (2009). Shakeout-d: Ground motion estimates using an ensemble of large earthquakes on the southern San Andreas fault with spontaneous rupture propagation. *Geophy. Res. Lett.*, 36(4).

Olsen, K. B., R. J. Archuleta, and J. R. Matarese (1995). Three-dimensional simulation of a magnitude 7.75 earthquake on the San Andreas fault. *Science*, 270(5242), 1628.

Pasyanos, M. E., H. Tkalčić, R. Gök, A. Al-Enezi, and A. J. Rodgers (2007). Seismic structure of Kuwait. *Geophys. J. Int.*, 170(1), 299–312.

Pitarka, A., K. Irikura, T. Iwata, and H. Sekiguchi (1998), Three-dimensional simulation of the near-fault ground motion for the 1995 Hyogo-Ken Nanbu (Kobe), Japan, earthquake, *Bull. Seismol. Soc. Am.*, 88(2), 428–440.

Pitarka, A., M. Pasyanos, R. Mellors, and A. Rodgers (2012). Observation and simulation of long-period ground motions in the Persian/Arabian Gulf from earthquakes in Zagros thrust belt. Tech. rep., Lawrence Livermore National Laboratory (LLNL), Livermore, CA.

Pitarka, A., A. Al-Amri, M. E. Pasyanos, A. J. Rodgers, and R. J. Mellors (2015). Long period ground motion in the Arabian Gulf from earthquakes in the Zagros mountains thrust belt. *Pure. and Appl. Geophy.*, 172(10), 2517–2532.

Prieto, G. A., and G. C. Beroza (2008). Earthquake ground motion prediction using the ambient seismic field, *Geophy. Res. Lett.*, 35(14).

Prieto, G. A., J. F. Lawrence, A. I. Chung, and M. D. Kohler (2010). Impulse response of civil structures from ambient noise analysis. *Bull. Seismol. Soc. Am.*, 100(5A), 2322–2328.

Rubinstein, J. L., and A. B. Mahani (2015). Myths and facts on wastewater injection, hydraulic fracturing, enhanced oil recovery, and induced seismicity, *Seismol. Res. Lett.*, 86, no. 4, 1060–1067.

Sadek, A. (2004). Seismic map for the State of Kuwait. *Emirates J. Eng. Res.*, 9(2), 53–58.

Sarkar, S. (2008). Reservoir monitoring using induced seismicity at a petroleum field in Oman, Ph.D. thesis, Massachusetts Institute of Technology.

Shapiro, S. A. (2015). Fluid-Induced Seismicity, Cambridge University Press.

Shakal, A. F., M. J. Huang, and R. B. Darragh (1996). Interpretation of significant ground-response and structure strong motions recorded during the 1994 Northridge earthquake. *Bull. Seismol. Soc. Am.*, 86(1B), S231-S246.

Şeşetyan, K., Danciu, L., Demircioğlu Tümsa, M.B. et al. (2018). The 2014 Earthquake Model of the Middle East: overview and results. *Bull Earthquake Eng*., 1-34

Snieder, R., and E. Sáfak (2006). Extracting the building response using seismic interferometry: Theory and application to the Millikan Library in Pasadena, California. *Bull. Seismol. Soc. Am.*, 96(2), 586–598.

Sun, H., A. Mordret, G. A. Prieto, M. N. Toksöz, and O. Büyüköztürk (2017). Bayesian characterization of buildings using seismic interferometry on ambient vibrations. *Mechanical Systems and Signal Processing*, 85, 468-486.

Talebian, M., & Jackson, J. (2004). A reappraisal of earthquake focal mechanisms and active shortening in the Zagros mountains of Iran. *Geophy. J. Int.*, 156(3), 506-526.

Zoback, M. D., and S. M. Gorelick (2012). Earthquake triggering and large-scale geologic storage of carbon dioxide, Proc. Natl. Acad. Sci., 109, no. 26, 10164–10168.

Table 1. Preferred 1-D elastic model (KUW-P) for ground motion calculation[a]

Layer number	Thickness (km)	V_P (km/s)	V_S (km/s)	Density (g/cm^2)	Q_P (s^{-1})	Q_S (s^{-1})
1	2.0	2.25	1.40	2.50	40	20
2	2.0	4.76	2.75	2.60	100	50
3	17.0	5.89	3.40	2.70	300	150
4	9.0	6.41	3.70	2.70	300	150
5	11.0	6.95	3.90	2.70	300	150
6	∞	7.80	4.40	2.70	300	150

[a]To better fit the observed seismograms, we varied the thickness, P-wave velocity (V_P), and S-wave velocity (V_S) of the first layer of the KUW1 model of Pasyanos et al. (2007).

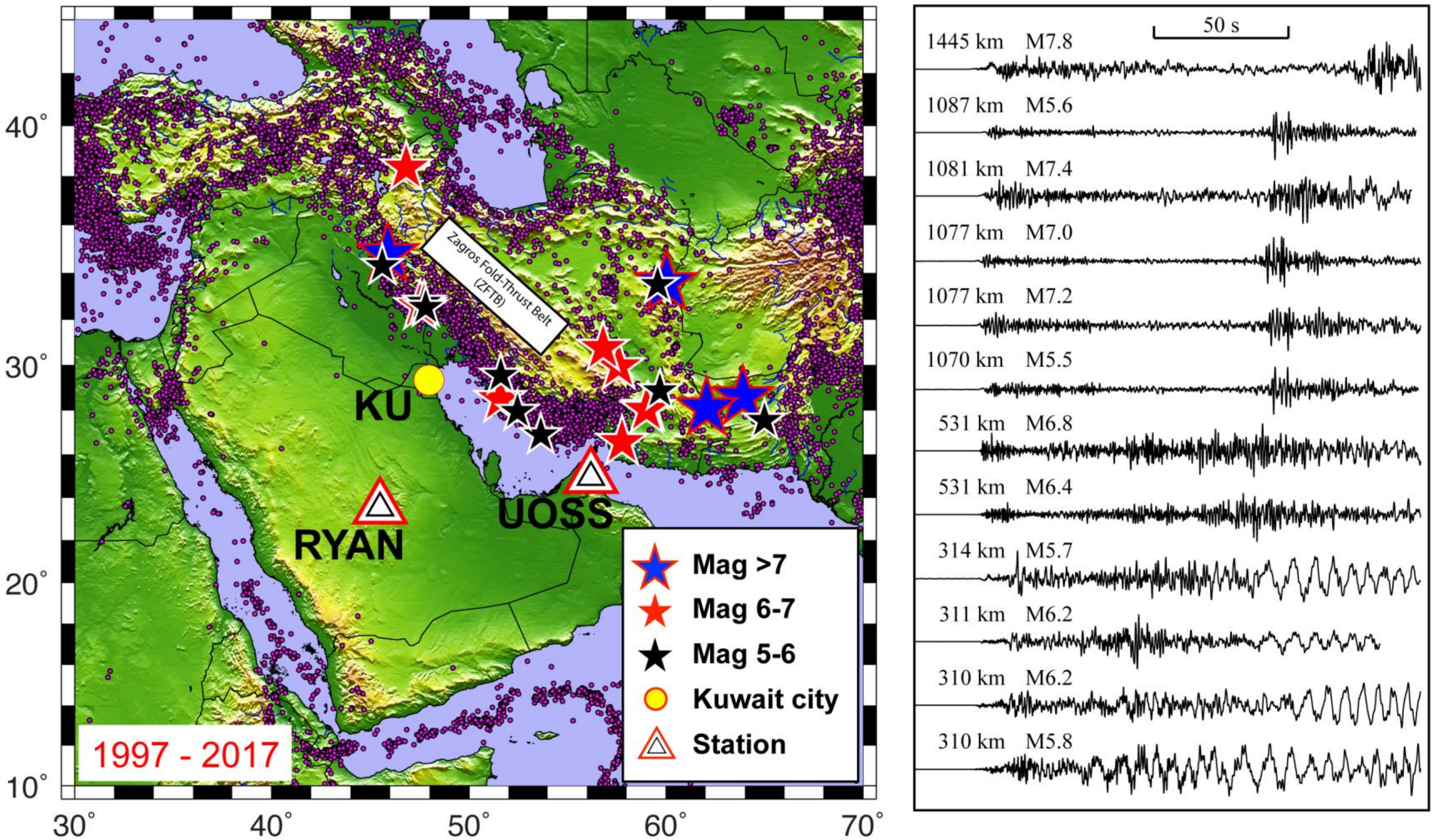

Figure 1. Significant regional earthquakes since 1997. Seismograms are recorded by the broadband station MI in Kuwait. Duration of recording is limited to 200 seconds for each event. For events farther than 300 km, surface waves are not recorded because the recordings are limited to 200 seconds and seismograms are truncated.

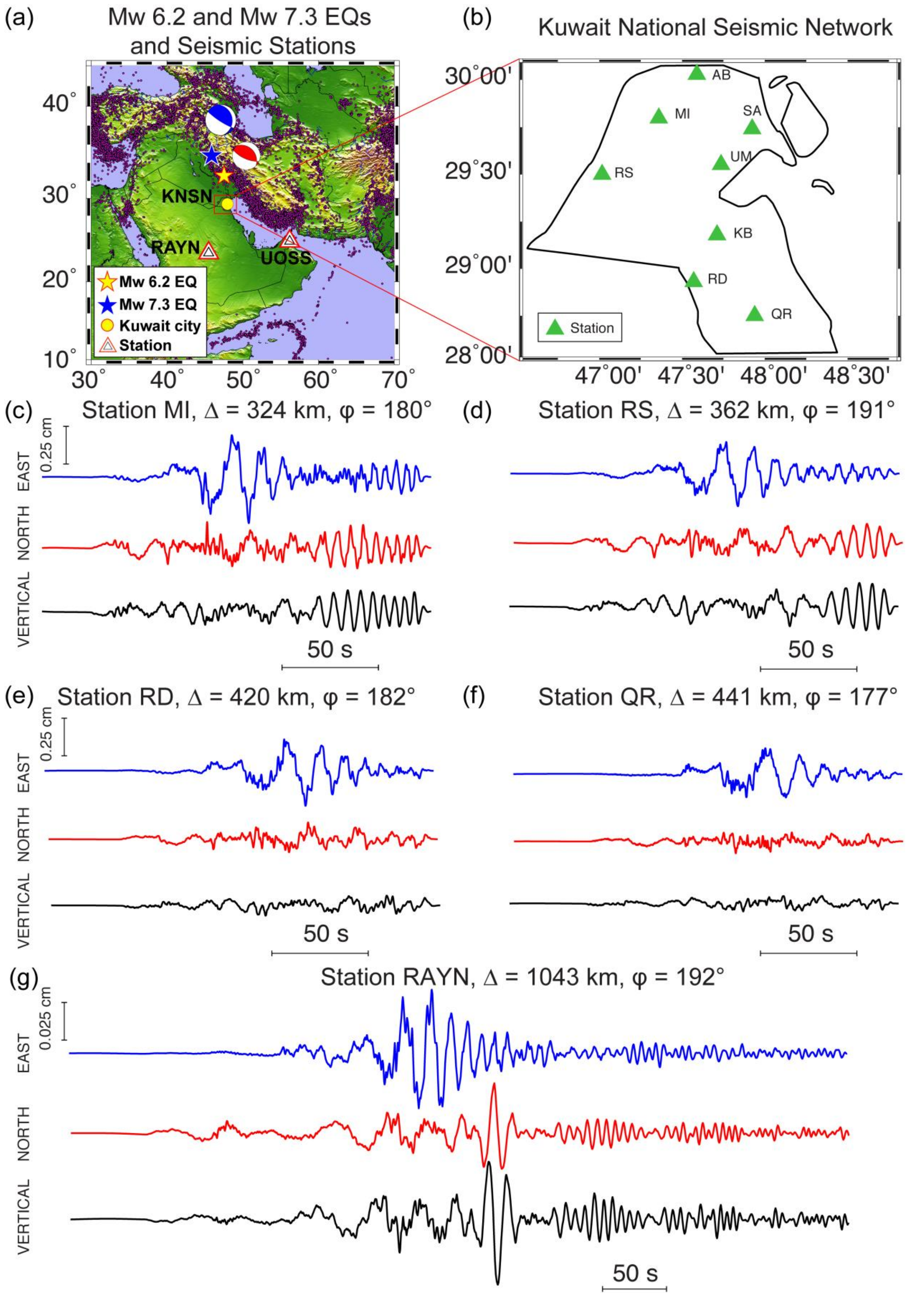
(a)
Mw 6.2 and Mw 7.3 EQs
and Seismic Stations
40°
30°
20°
10°
30°
40°
50°
60°
70°
KNSN
RAYN
UOSS
Mw 6.2 EQ
Mw 7.3 EQ
Kuwait city
Station
(b)
Kuwait National Seismic Network
30°00'
29°30'
29°00'
28°00'
47°00'
47°30'
48°00'
48°30'
AB
MI
SA
UM
RS
KB
RD
QR
Station
(c)
Station MI, Δ = 324 km, φ = 180°
(d)
Station RS, Δ = 362 km, φ = 191°
0.25 cm
EAST
NORTH
VERTICAL
50 s
50 s
(e)
Station RD, Δ = 420 km, φ = 182°
(f)
Station QR, Δ = 441 km, φ = 177°
0.25 cm
EAST
NORTH
VERTICAL
50 s
50 s
(g)
Station RAYN, Δ = 1043 km, φ = 192°
0.025 cm
EAST
NORTH
VERTICAL
50 s

Figure 2. (a) The 2014/08/18 Mw 6.2 and 2017/11/12 Mw 7.3 earthquakes and seismic stations in a geographic map. The yellow and blue stars show the hypocenters of the Mw 6.2 and Mw 7.3 earthquakes, the yellow circle shows Kuwait City, the red rectangle shows the region covered by Kuwait National Seismic Network (KNSN), the white triangles show station RAYN in Saudi Arabia and station UOSS in UAE and the red and blue beach balls show the source mechanism of the Mw 6.2 and Mw 7.3 earthquake. This earthquake was widely felt in Kuwait. (b) The eight stations of KNSN throughout Kuwait. The five broadband Stations MI, QR, RD, RS and UM were operational when the Mw 6.2 earthquake occurred. (c) The observed seismograms of Mw 6.2 earthquake at MI in Kuwait. Since the epicenter is north of the station, the Z and N component seismograms are alike, mostly Rayleigh waves. The E component is primarily Love waves. (d)-(f) The three-component seismograms of Mw 6.2 earthquake at station RS, RD and QR. Because all the stations of KNSN are to the south of the hypocenter of Mw 6.2 earthquake, all the waveforms are very similar showing very consistent Love and Rayleigh waves. The Rayleigh waves of RD and QR are truncated because of the 200 sec recording limits (g) The three-component seismograms of stations RAYN. Because RAYN is almost to the south of the hypocenter of Mw 6.2 earthquake, the seismograms show similar Love and Rayleigh waves as stations of KNSN.

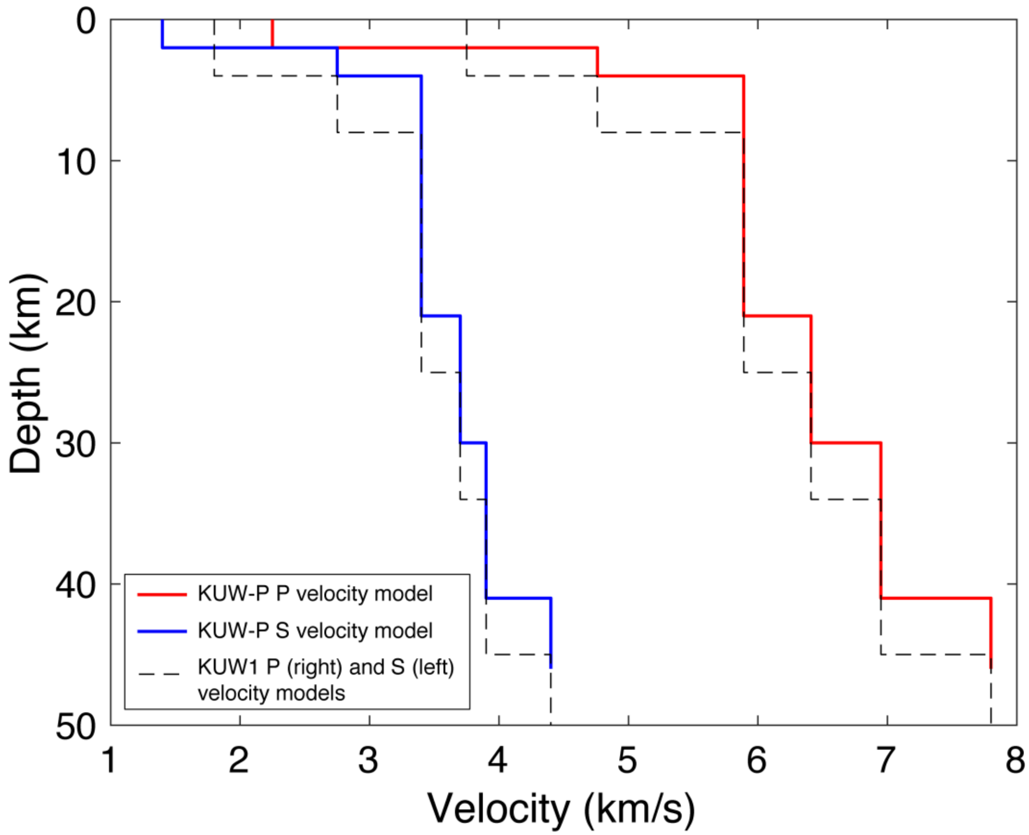

Figure 3. The comparison of the KUW1 and the preferred velocity (KUW-P) models. The red and blue lines show the P and S velocities of the KUW-P model. The black dashed line denotes the KUW1 P (right) and S (left) velocity models.

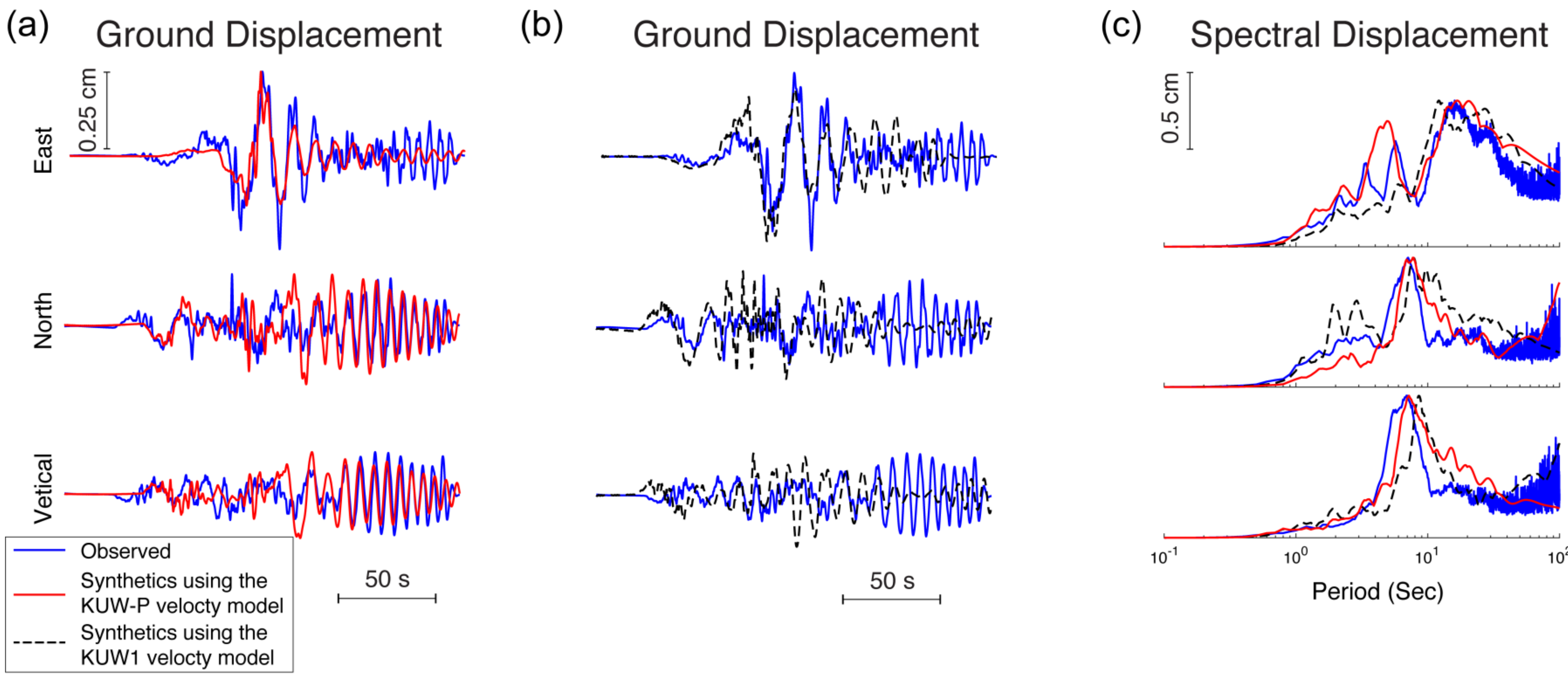

Figure 4. The observed and modeled ground displacement and spectral displacement of the 08/18/2014 Mw 6.2 earthquake at MI. (a) The blue lines show the observed seismograms and the red lines show the synthetic seismograms using the KUW-P velocity model, (b) The blue lines show the observed seismograms and the dashed black lines show the synthetic seismograms using the KUW1 velocity model. (c) The blue lines show the observed

spectral displacement, the red lines show synthetic spectral displacement using the preferred velocity model, and the dashed black lines show the synthetic seismograms using the KUW1 velocity model.

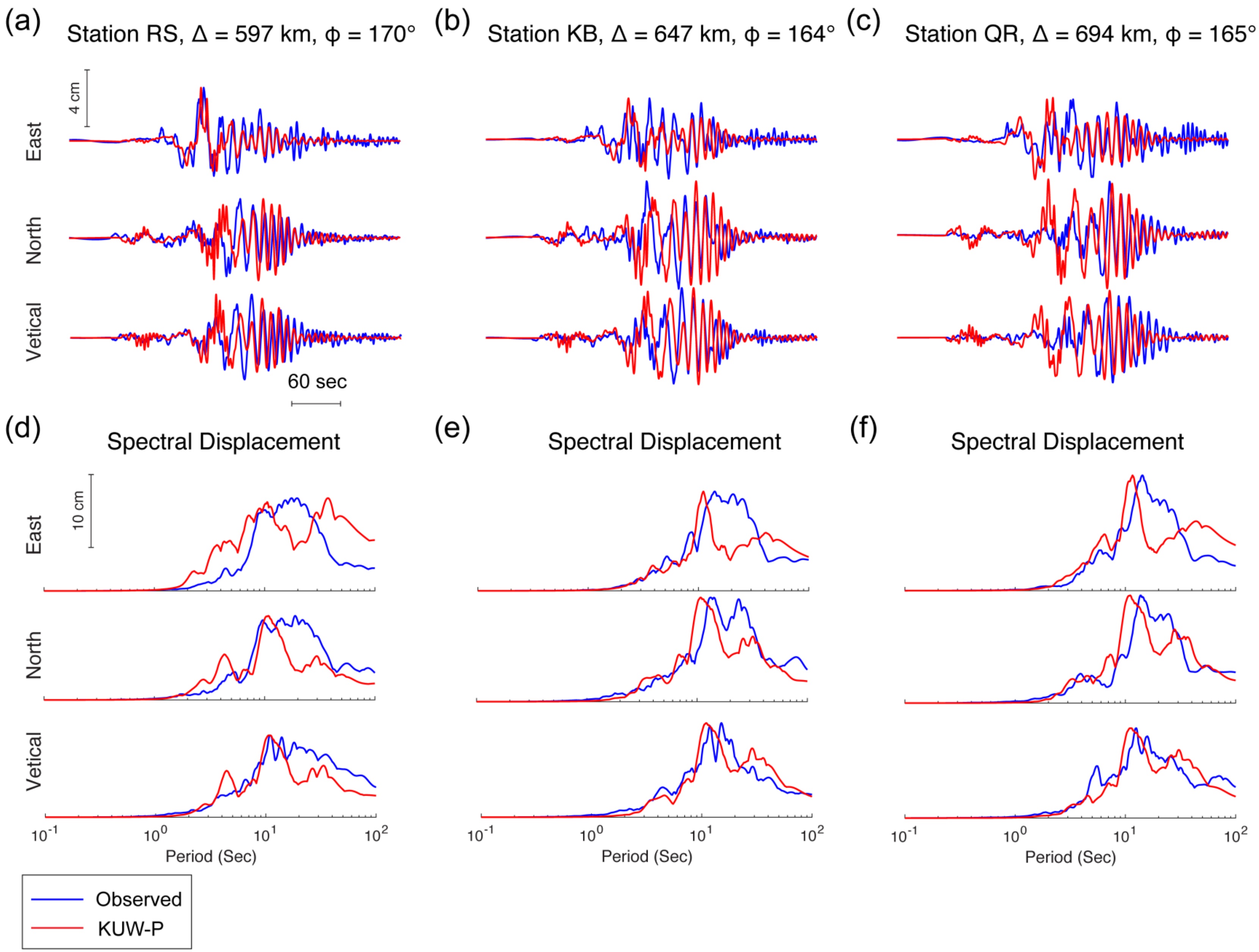

(a)
Station RS, Δ = 597 km, ϕ = 170°
(b)
Station KB, Δ = 647 km, ϕ = 164°
(c)
Station QR, Δ = 694 km, ϕ = 165°
4 cm
East
North
Vetical
60 sec
(d)
Spectral Displacement
(e)
Spectral Displacement
(f)
Spectral Displacement
10 cm
East
North
Vetical
10^-1
10^0
10^1
10^2
Period (Sec)
Observed
KUW-P

450

Figure 5. The comparison of the observed (blue) and modeled (red) ground displacement and spectral displacement of the 11/12/2017 Mw 7.3 earthquake at stations KB, QR and RS using the KUW-P. (a)-(c) 3-Component displacement seismograms. (d)-(f) 3-Component spectral displacements.

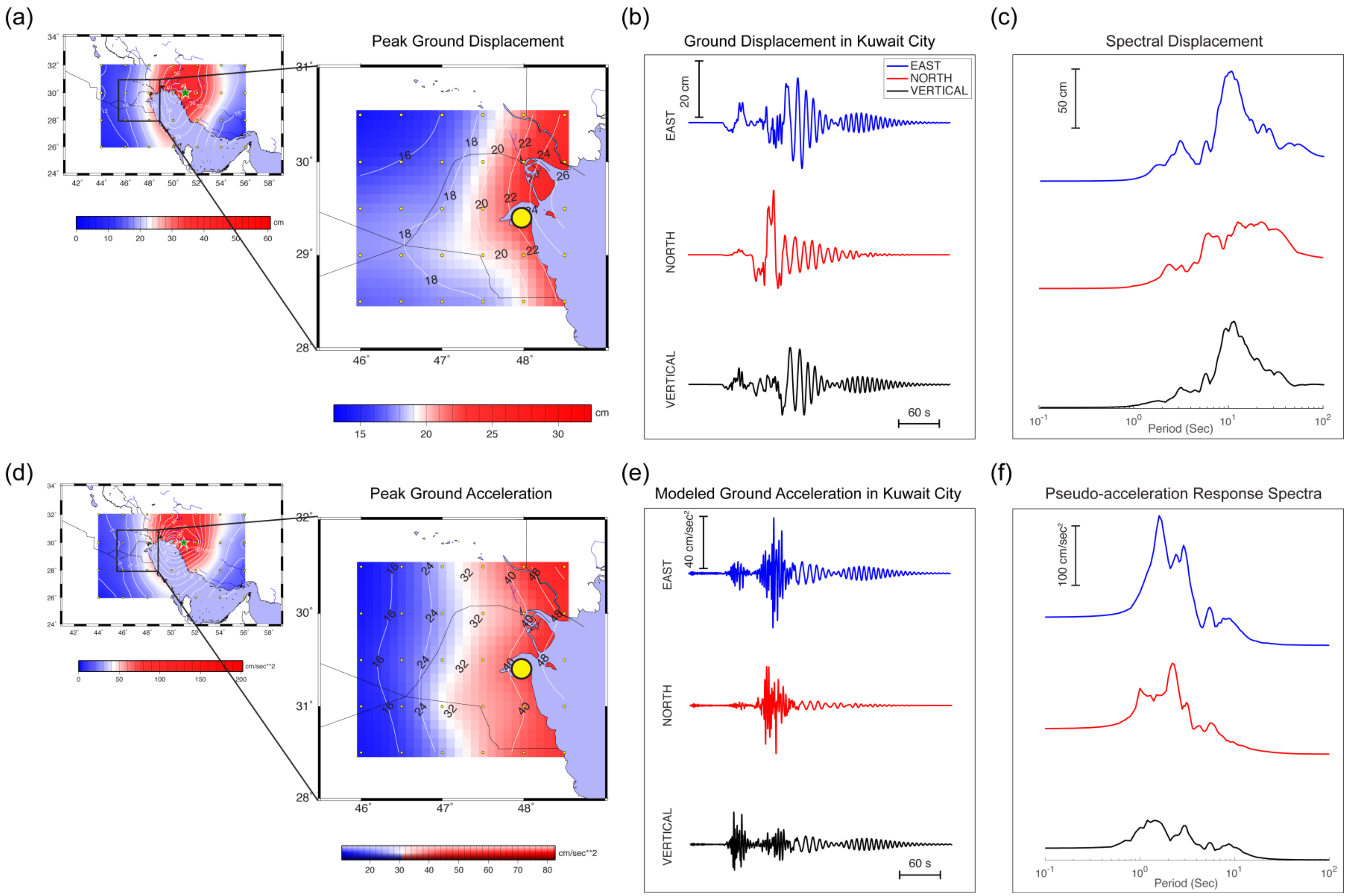
(a)
Peak Ground Displacement
cm
(b)
Ground Displacement in Kuwait City
EAST
NORTH
VERTICAL
20 cm
60 s
(c)
Spectral Displacement
50 cm
Period (Sec)
(d)
Peak Ground Acceleration
cm/sec**2
(e)
Modeled Ground Acceleration in Kuwait City
EAST
NORTH
VERTICAL
40 cm/sec²
60 s
(f)
Pseudo-acceleration Response Spectra
100 cm/sec²
Period (Sec)

Figure 6. Modeled ground motions in Kuwait City (yellow circle) due to magnitude Mw=7.5 thrust earthquake in Zagros with strike = 300°, Dip=20°, and Rake=90°. (a) The contour of peak ground displacement (PGD; cm) in the north-south direction around the epicenter (green star); (b) the 3-component displacement (cm) at Kuwait City; (c) the spectral displacement (cm); (d) the contour of peak ground accelerations (PGA; cm/s^2) in the north-south direction around the epicenter (green star); (e) the 3-component acceleration (cm/s^2) at Kuwait City; (f) the pseudo-acceleration response spectra (cm/s^2).

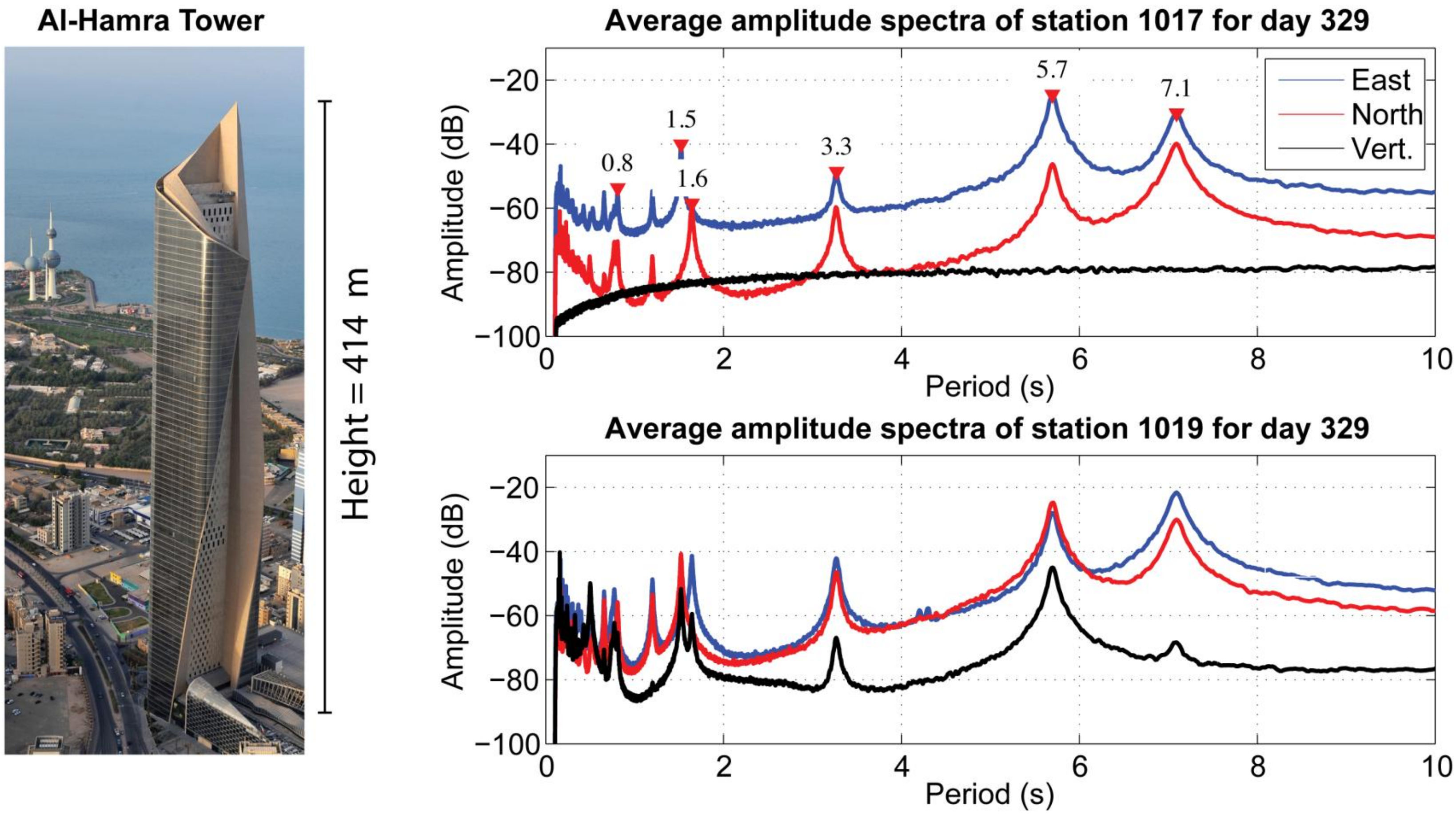

Figure 7. Amplitude spectra, calculated using ambient vibrations data recorded by two Kinemetrics EpiSensor instruments, at the top of the Al-Hamra Tower. Average spectra for the day 329 were computed with a 600 s moving window. The vertical component of station 1017 was not working.

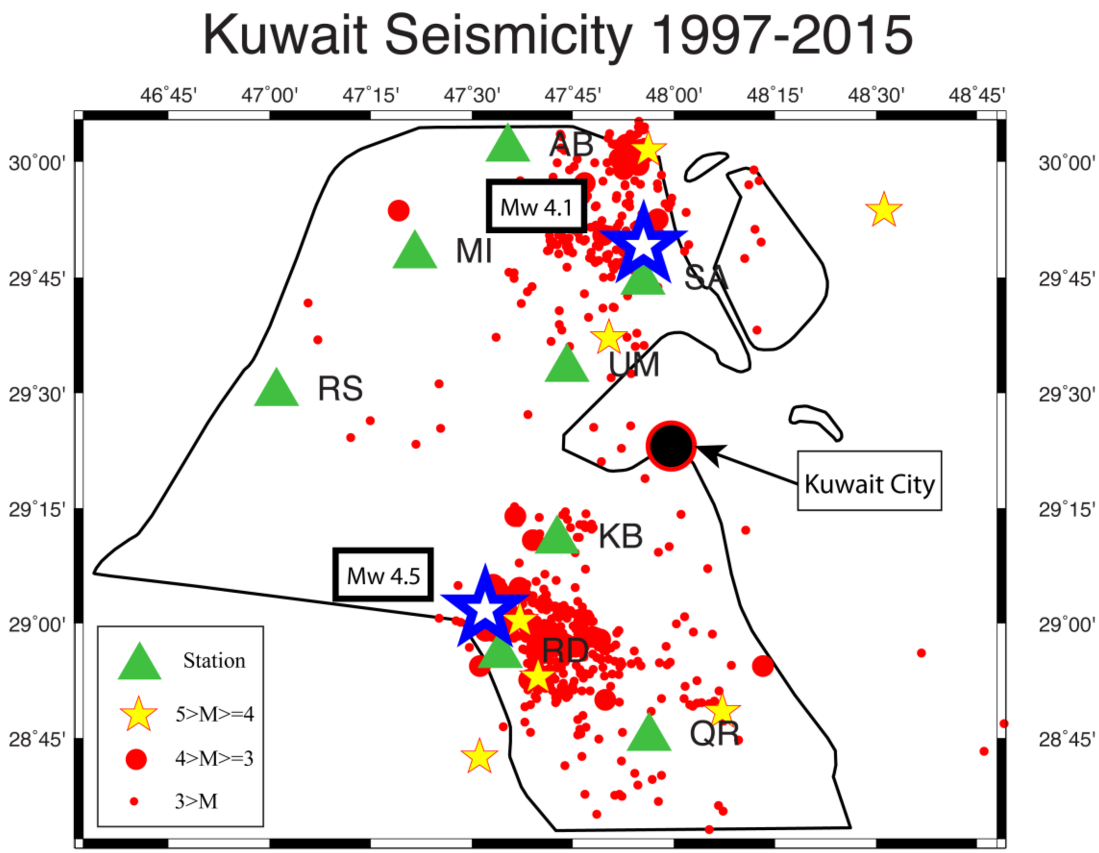

Figure 8. Local earthquakes (left) during 1997 to 2015 in Kuwait. We show earthquakes with M ≥ 4 as yellow stars, 4 > M ≥ 3 as large red circles, and M < 3 in small red circles. The 03/21/2015 Mw 4.5 and 08/18/2015 Mw 4.1 earthquakes are marked as blue stars.

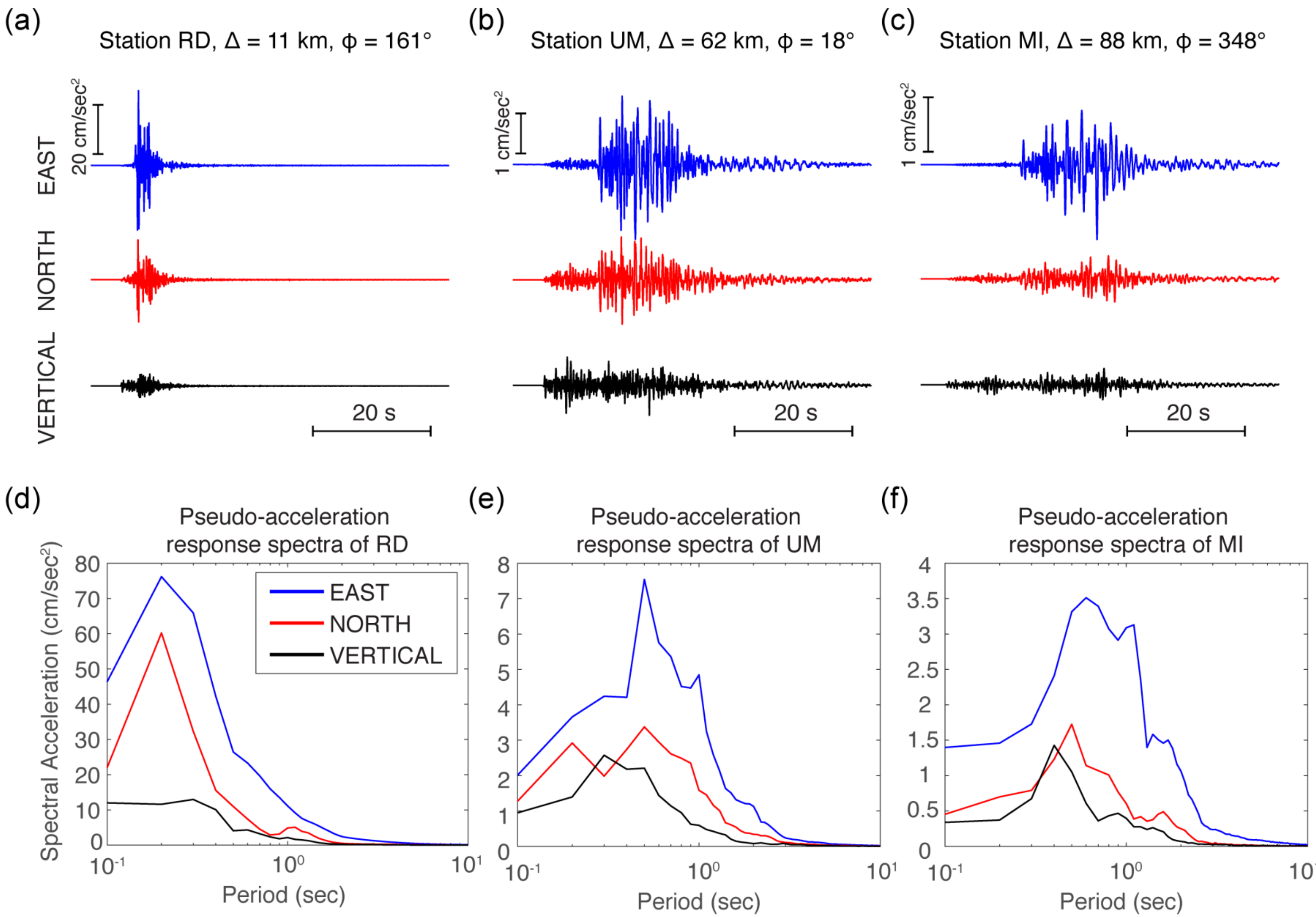

(a)
Station RD, Δ = 11 km, ϕ = 161°
(b)
Station UM, Δ = 62 km, ϕ = 18°
(c)
Station MI, Δ = 88 km, ϕ = 348°
EAST
NORTH
VERTICAL
20 cm/sec²
1 cm/sec²
1 cm/sec²
20 s
20 s
20 s
(d)
Pseudo-acceleration response spectra of RD
(e)
Pseudo-acceleration response spectra of UM
(f)
Pseudo-acceleration response spectra of MI
Spectral Acceleration (cm/sec²)
EAST
NORTH
VERTICAL
Period (sec)
Period (sec)
Period (sec)

Figure 9. (a)-(c) 3-Component acceleration seismograms for the Mw 4.5 local event (from Kuwait National Seismic Network stations. (d)-(f) Pseudo-acceleration response spectra of 3-Component seismograms for the Mw 4.5 local event (from Kuwait National Seismic Network stations).

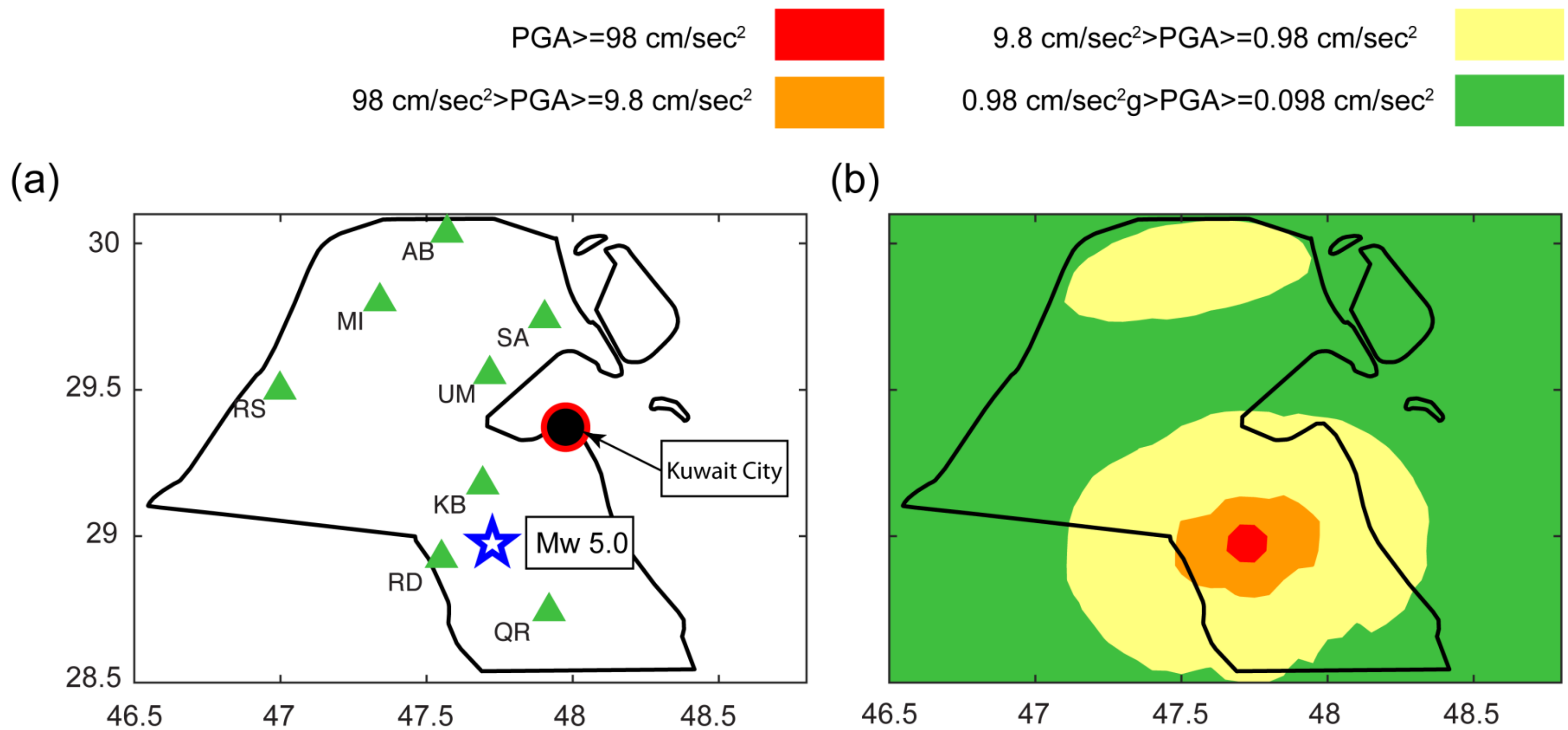

Figure 10. (a) The location of the modeled Mw 5.0 local earthquake (blue star). (b) The contour of peak ground acceleration (PGA; cm/sec^2) around the epicenter (blue star). We generate the synthetic acceleration seismograms in the map region for this Mw 5.0 earthquake, a thrust event with fault plane: strike = 85°, dip = 20°, and rake = 10°. The PGAs are calculated from the acceleration seismograms.